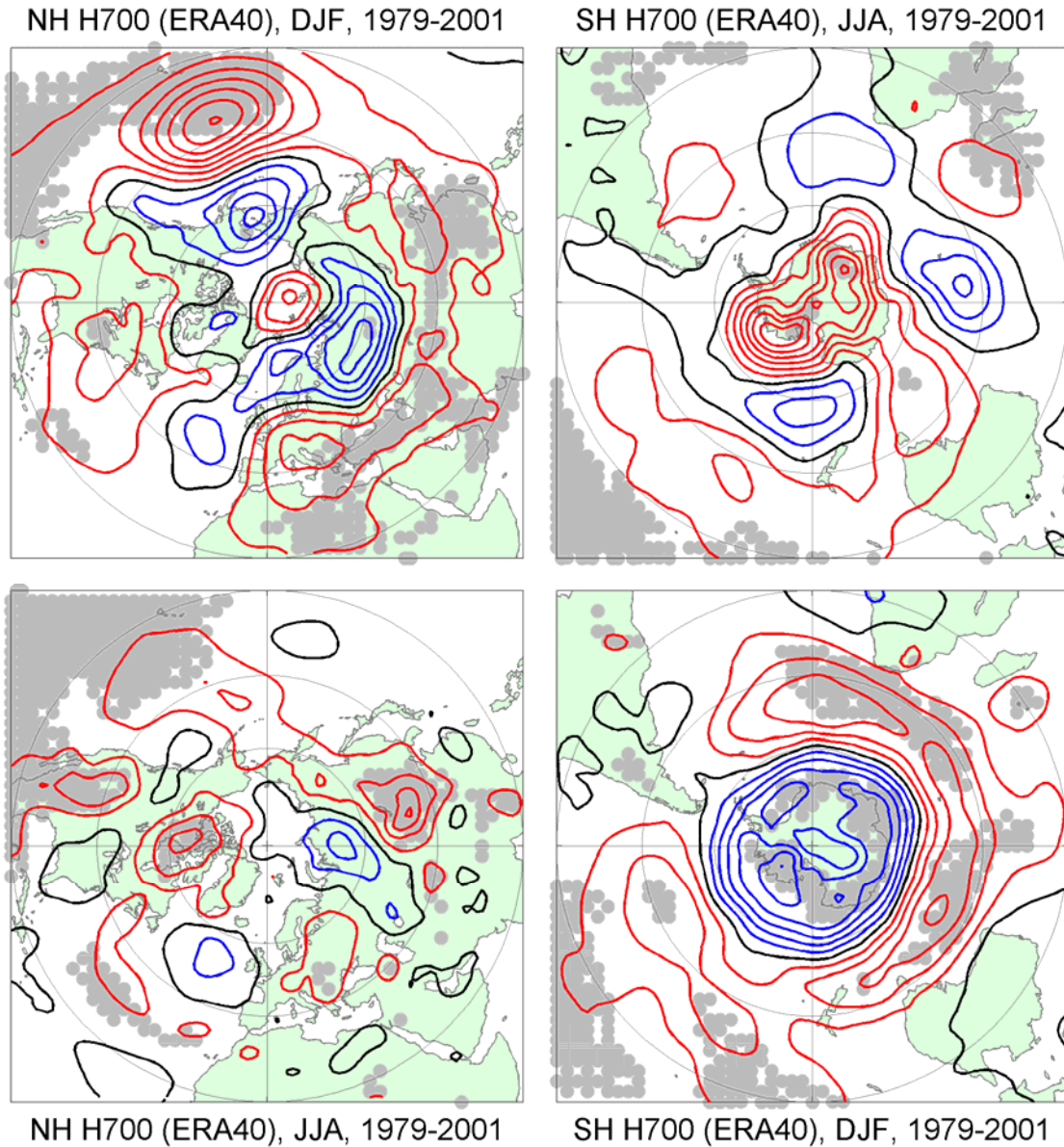


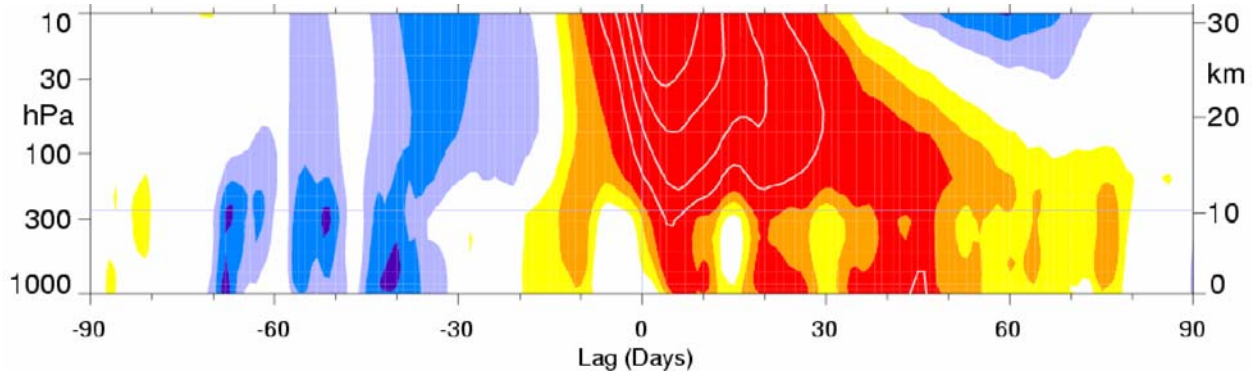
1



2
3
4
5
6
7
8
9

Figure 3.5.1. Linear trends in ERA-40 700 hPa geopotential height, 1979–2001 for DJF for (top left and bottom right) and JJA (bottom left and top right), for the NH (left) and SH (right). Trends are contoured in 5 gpm decade⁻¹ and are calculated from seasonal means of daily 1200 UTC fields. Red contours are positive, blue negative, and black zero; the grey background indicates 1% statistical significance using a standard least-squares F-test and assuming independence between years.

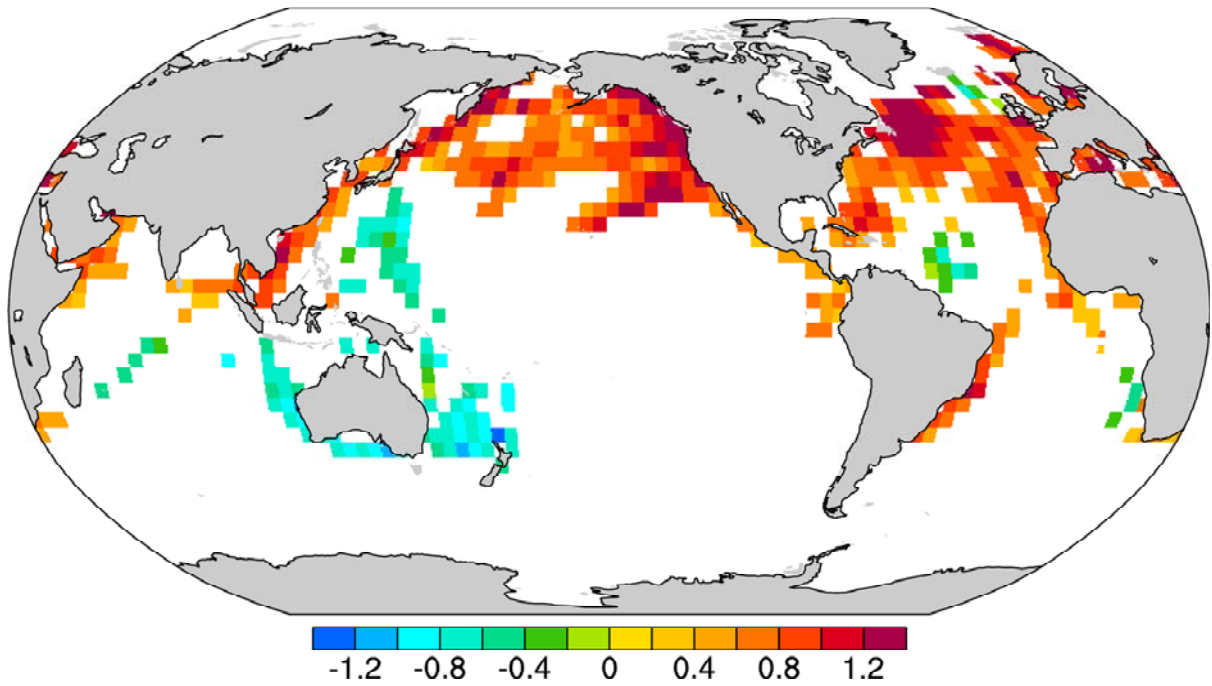
1
2



3
4
5
6
7
8
9
10
11
12

Box 3.3, Figure 3.5.2. Composites of time-height development of the NAM index for 18 weak vortex events. The events are selected by the dates on which the 10 hPa annular mode index crossed -3.0 . Day 0 is the start of the weak vortex event. The indices are nondimensional; the contour interval for the colour shading is 0.25, and 0.5 for the white contours. Values between -0.25 and 0.25 are not shaded. Yellow and red shading indicates negative NAM indices and blue shading indicates positive indices. The thin horizontal lines indicate the approximate boundary between the troposphere and the stratosphere. Modified from Baldwin and Dunkerton (2001).

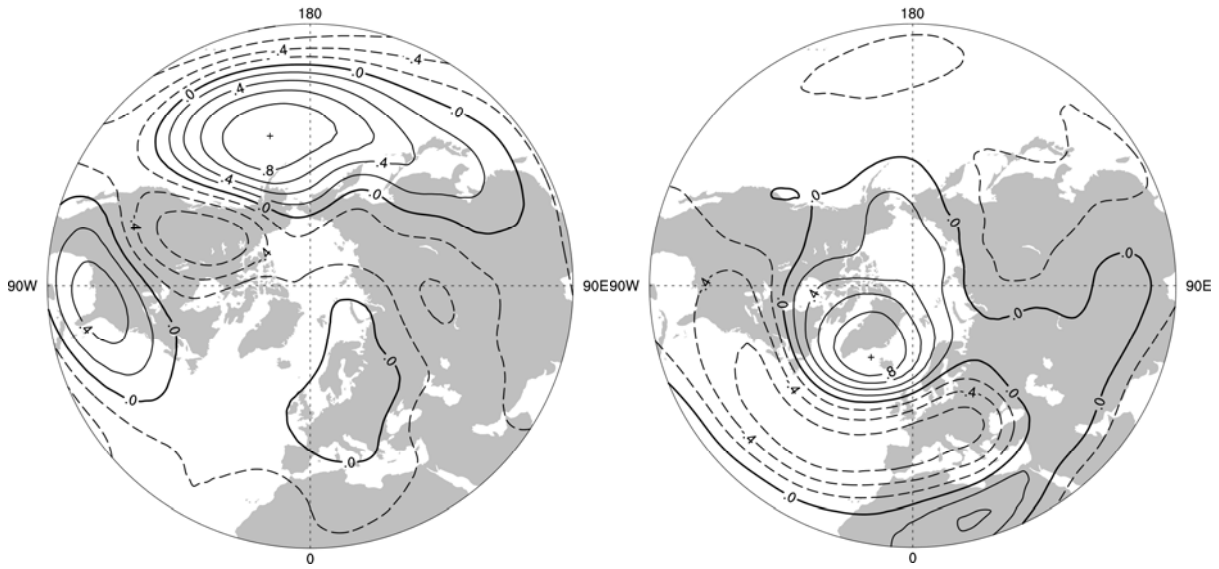
1
2



3
4
5
6
7
8
9

Figure 3.5.3. Estimates of linear trends in significant wave height (cm decade⁻¹) for the regions along the major ship routes for the global ocean for the period 1950–2002. Trends are shown only for the locations where they are significant at the 95% level. Adapted from Gulev and Grigorieva (2004).

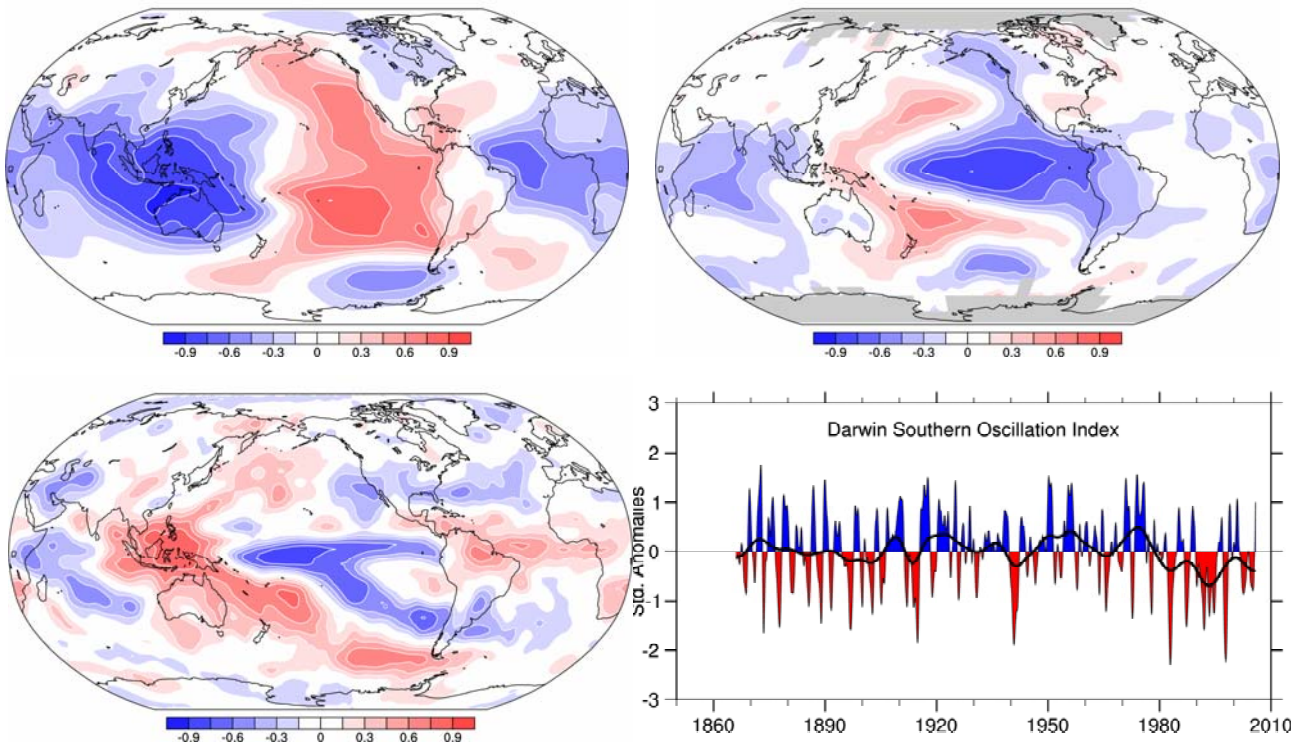
1
2
3



4
5
6
7
8
9
10
11

Figure 3.6.1. The PNA (left) and NAO (right) teleconnection patterns, shown as one-point correlation maps of 500 hPa geopotential heights for boreal winter (DJF) over 1958–2005. In the left panel, the reference point is 45°N, 165°W, corresponding to the primary centre of action of the PNA pattern, given by the + sign. In the right panel, the NAO pattern is illustrated based on a reference point of 65°N, 30°W. Negative correlation coefficients are dashed, and the contour increment is 0.2. Adapted from Hurrell et al. (2003).

1
2

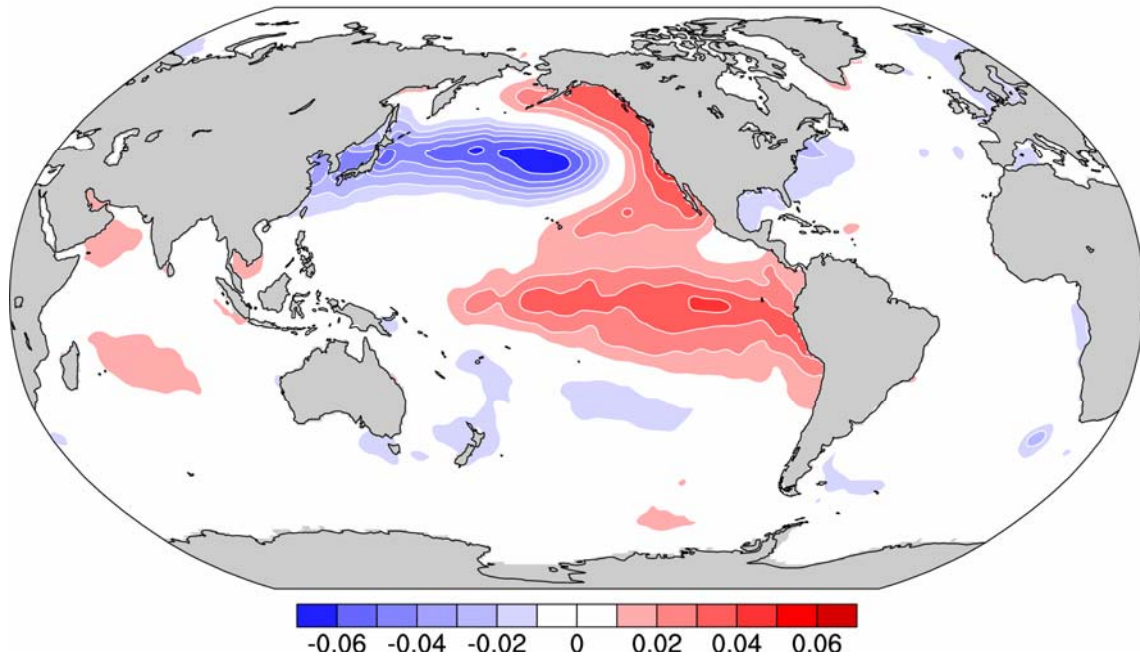


3
4
5
6
7
8
9
10
11
12

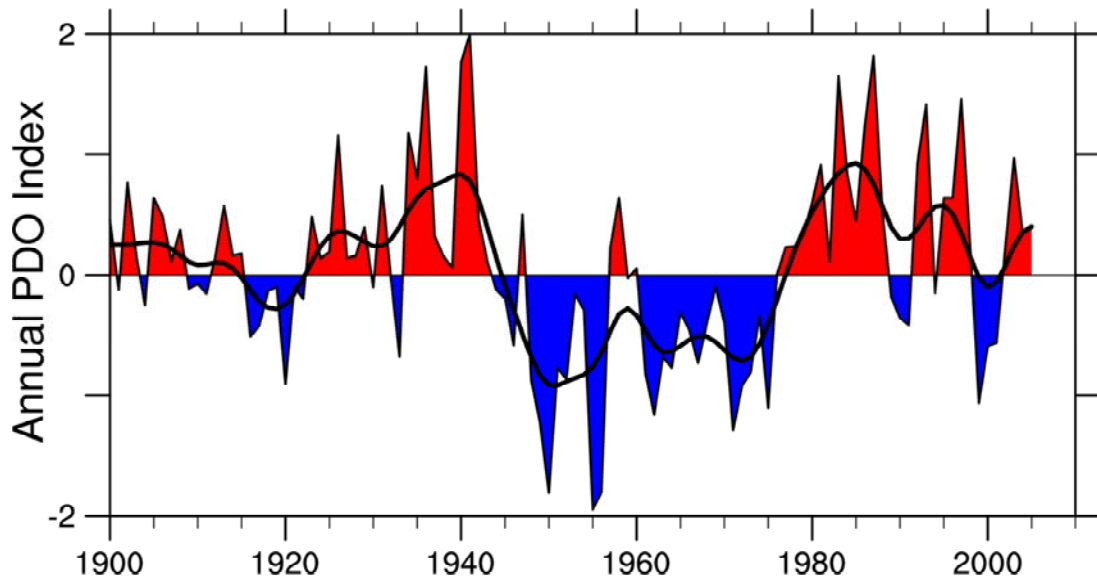
Figure 3.6.2. Correlations with the SO index (SOI), based on normalised Tahiti minus Darwin sea level pressures, for annual (May to April) means for sea level pressure (top left) and surface temperature (top right) for 1958–2004, and GPCP precipitation for 1979–2003 (bottom left) updated from Trenberth and Caron (2000). The Darwin-based SOI from 1866–2005 (Können et al 1998; lower right) features monthly values with an 11-point low pass filter, which effectively removes fluctuations with periods of less than 8 months (Trenberth, 1984). The thick black line represents the decadal filter (Appendix 3.A). Red values indicate positive sea level pressure anomalies at Darwin and thus El Niño conditions.

1
2

SST Anomalies: projected EOF 1: 20.8%



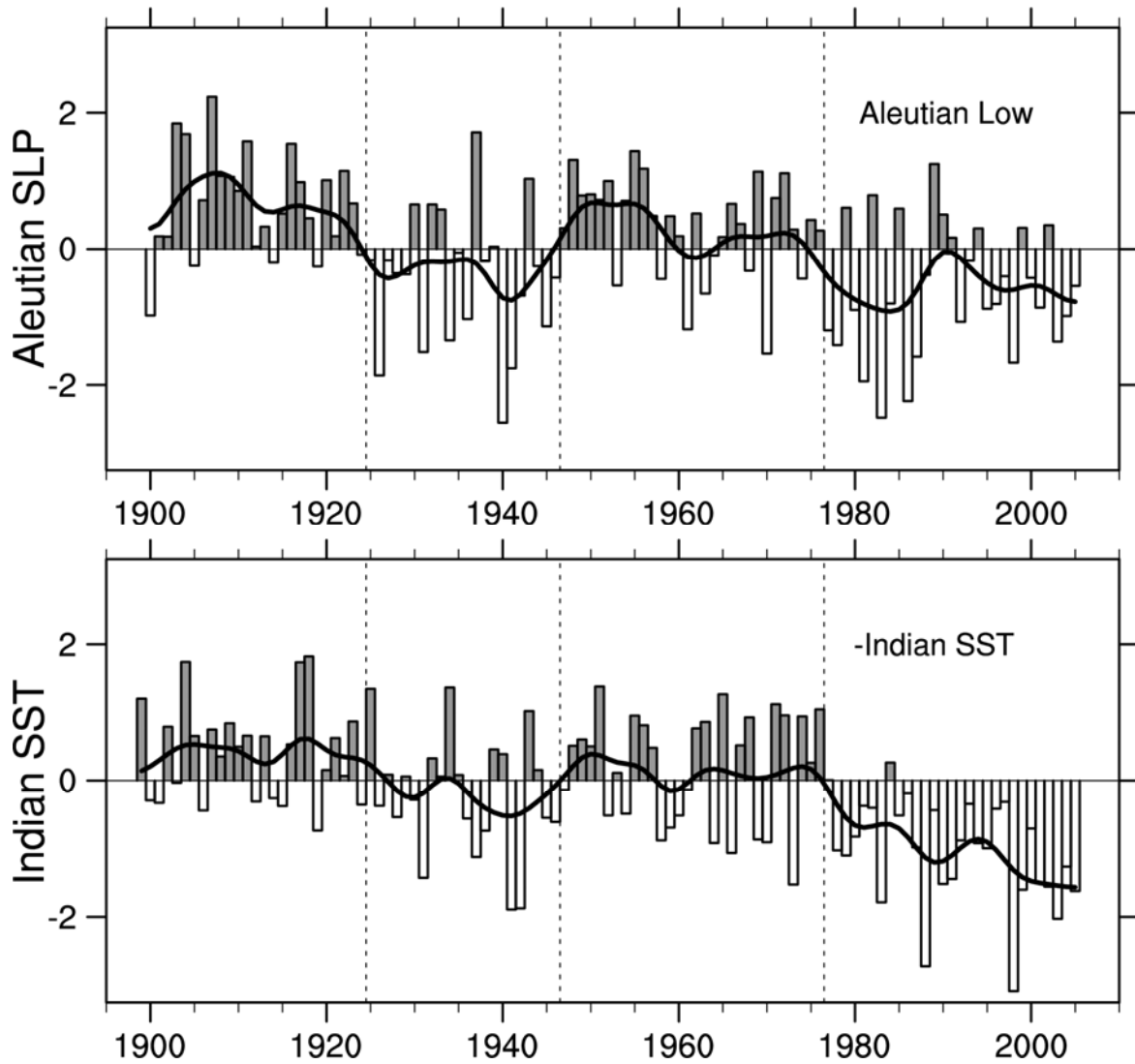
3



4
5
6
7
8
9
10
11

Figure 3.6.3. Pacific Decadal Oscillation. (a) SST based on the leading EOF SST pattern for the Pacific basin north of 20°N for 1911 to 2004 (updated; see Mantua et al., 1997; Power et al., 1999b) and projected for the global ocean (units are nondimensional); and (b) annual time series (updated from Mantua et al., 1997); the thick black curve uses the decadal filter (Appendix 3.A).

1
2

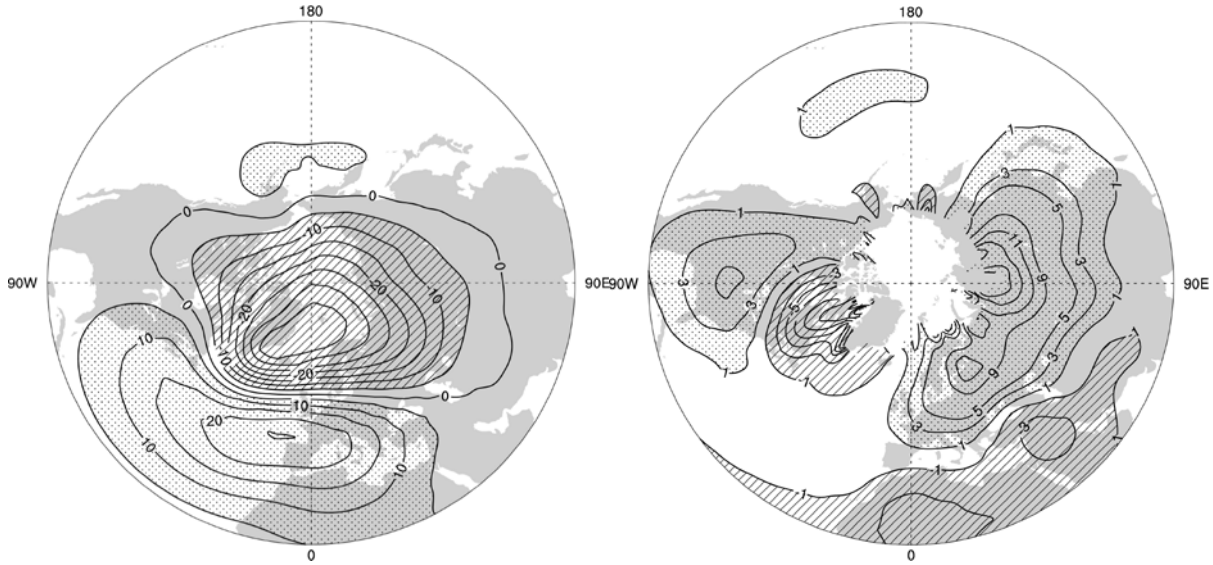


3

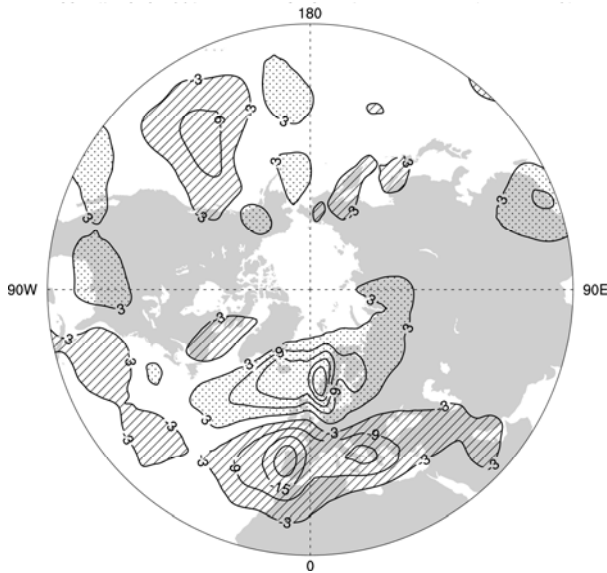
4
5
6
7
8
9
10
11
12
13
14
15
16

Figure 3.6.4. Top: Time series of the NPI (sea level pressure during December–March averaged over the North Pacific 30–65°N, 160°E–140°W) from 1900 to 2005 expressed as normalized departures from the long-term mean (each tick mark on the ordinate represents two standard deviations, or 2.8 hPa). This record reflects the strength of the wintertime Aleutian Low Pressure System, with positive (negative) values indicative of a weak (deep) Aleutian Low. The bars give the wintertime series and the thick curve is the decadal low-pass filter (Appendix 3.A). Values were updated and extended to earlier decades from Trenberth and Hurrell (1994). Lower: As above but for SSTs averaged over the Tropical Indian Ocean (10°S–20°N, 50–125°E; one standard deviation equals 0.18°C). This record has been inverted to facilitate comparison with (a). The dashed vertical lines mark years of transition in the Aleutian Low record (1925, 1947, 1977). Updated from Deser et al. (2004).

1
2



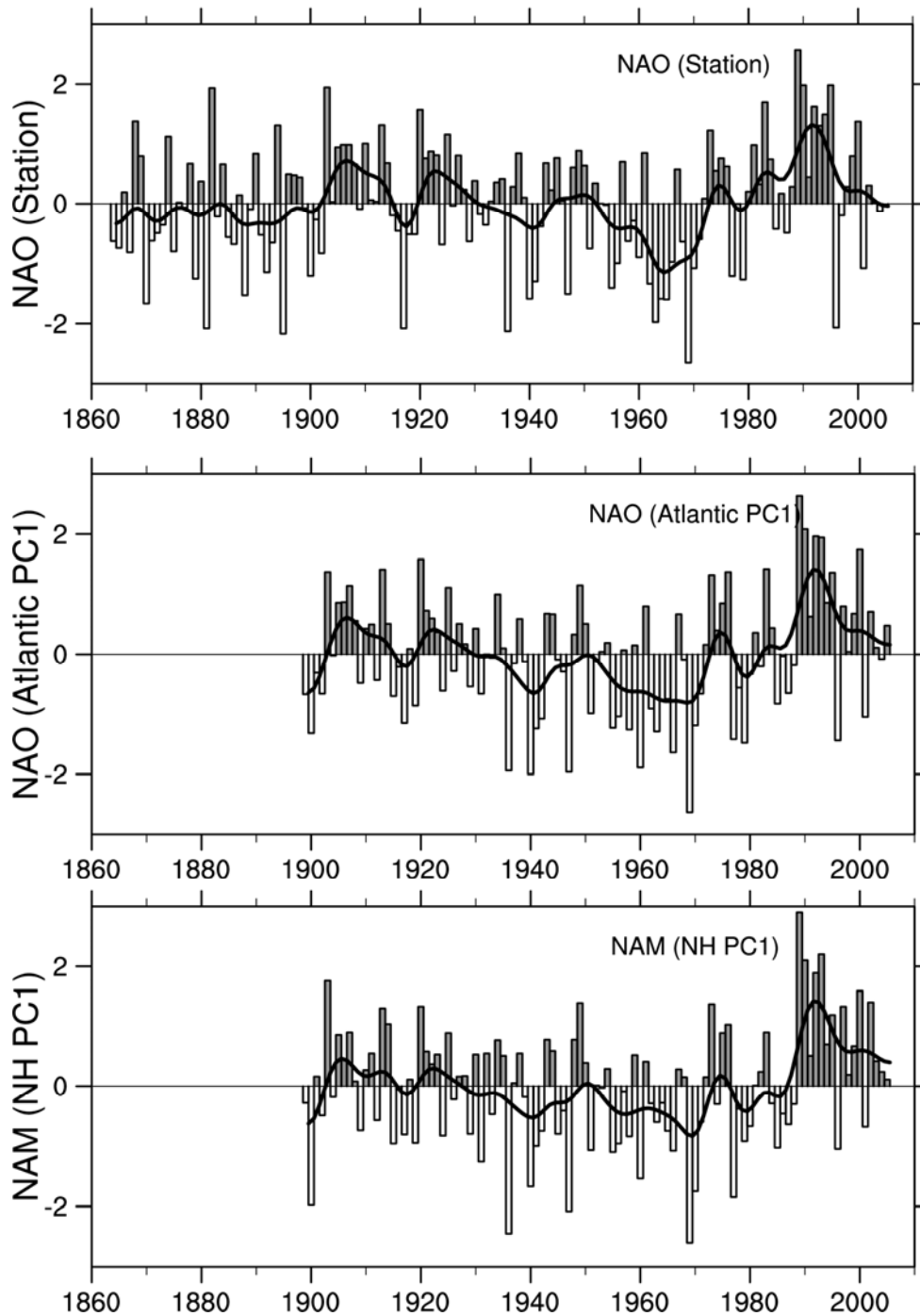
3
4



5
6
7
8
9
10
11
12
13
14
15

Figure 3.6.5. Changes in winter (December–March) corresponding to a unit deviation of the NAO index over 1900–2005 for (top left) mean sea level pressure in ($\times 10^{-1}$ hPa). Values greater than 0.5 hPa are stippled and < -0.5 hPa are hatched. (Top right) land surface air and sea surface temperatures ($\times 10^{-1}$ °C). The contour increment is 0.2°C. Temperature changes > 0.1 °C are indicated by stippling, and those < -0.1 °C are indicated by hatching. Regions of insufficient data (e.g., over much of the Arctic) are not contoured. (Bottom left) Precipitation for 1979–2003 based on GPCP ($\times 10^{-1}$ mm/day). Stippling indicates values > 0.3 mm/day and hatching values less than -0.3 mm/day. Contour interval 0.6 mm/day. Adapted from Hurrell et al. (2003).

1



2

3

4

5

6

7

8

9

10

11

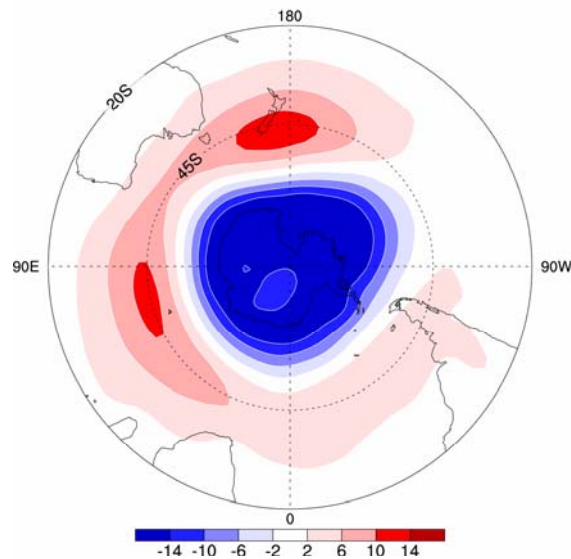
12

13

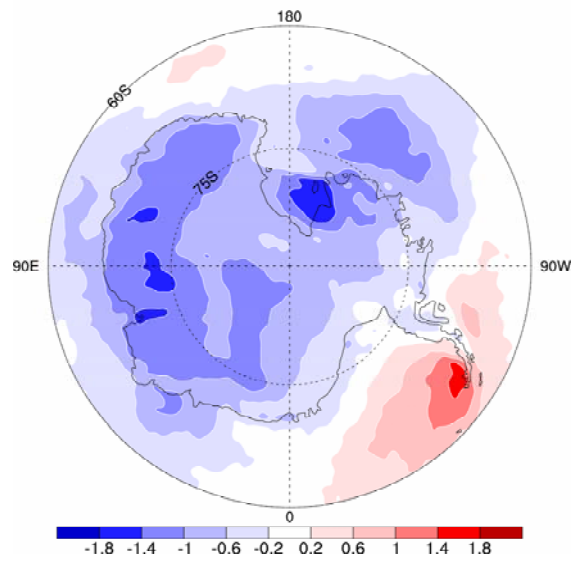
14

Figure 3.6.6. Normalized indices of the mean winter (December–March) NAO developed from sea level pressure data. In the top panel, the index is based on the difference of normalized sea level pressure between Lisbon, Portugal and Stykkisholmur/Reykjavik, Iceland from 1864 through 2005. The average winter sea level pressure data at each station were normalized by division of each seasonal pressure by the long-term (1864–1983) standard deviation. In the middle panel, the index is the principal component time series of the leading empirical orthogonal function (EOF) of Atlantic-sector sea level pressure. In the lower panel, the index is the principal component time series of the leading EOF of NH sea level pressure. The heavy solid lines represents the decadal filter (Appendix 3.A). The individual bar corresponds to the January of the winter season (e.g., 1990 is the winter of 1989/1990). See <http://www.cgd.ucar.edu/~jhurrell/nao.html> for updated time series. Updated from Hurrell et al. (2003).

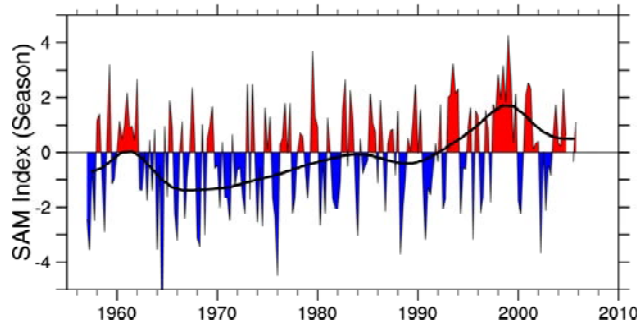
1



2



3



4

5

6

7

8

9

10

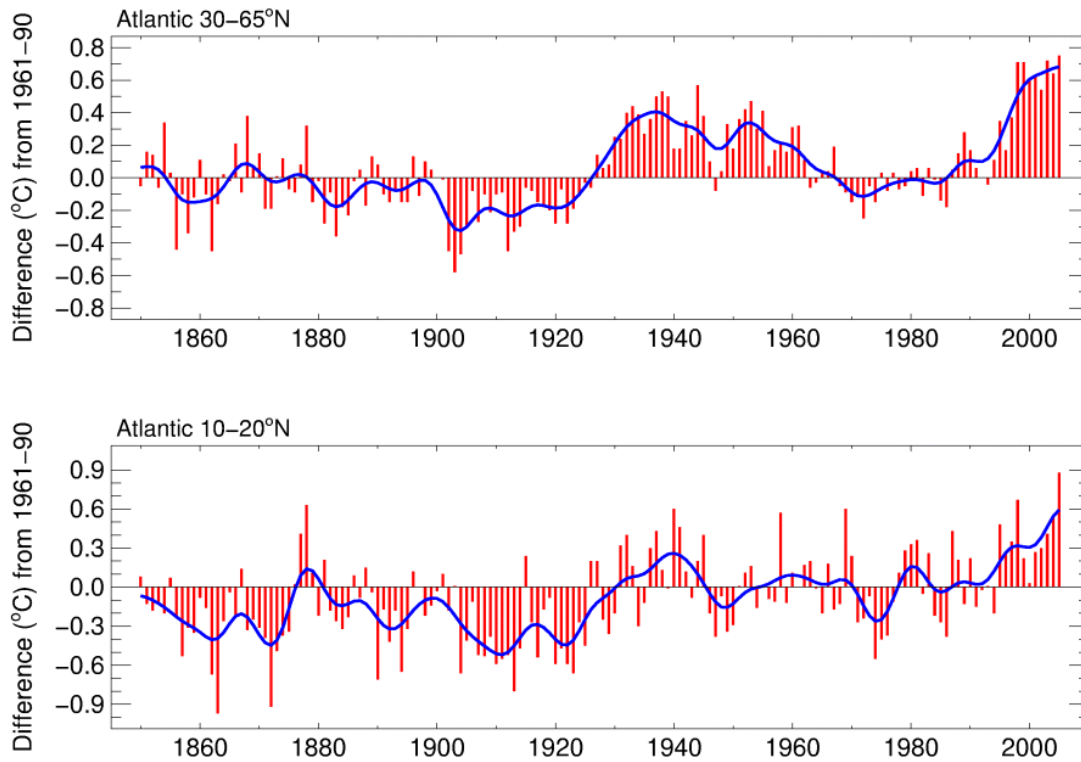
11

12

13

Figure 3.6.7. Bottom: Seasonal values of the SAM index calculated from station data (updated from Marshall, 2003). The thick black line is the decadal filter (Appendix 3.A). Top: SAM geopotential height pattern as a regression based on the SAM time series for seasonal anomalies at 850 hPa (see also Thompson and Wallace, 2000). Middle: the regression of changes in surface temperature (°C) over the 23-year period (1982–2004) corresponding to a unit change in the SAM index, plotted south of 60°S. Values exceeding about 0.4°C in magnitude are significant at the 1% confidence level (adapted from Kwok and Comiso, 2002b).

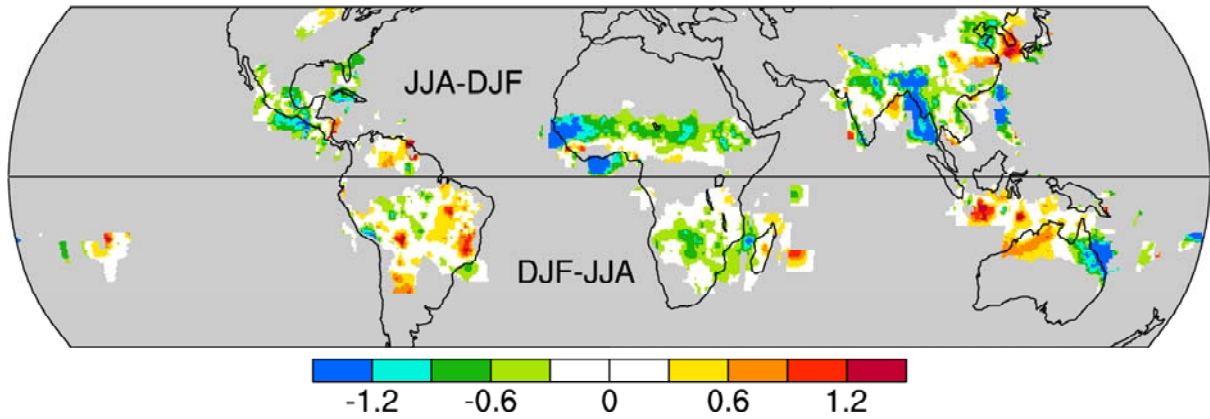
1
2



3
4
5
6
7
8
9

Figure 3.6.8. Atlantic Multidecadal Oscillation index 1850–2005 represented by annual anomalies of SST in the extratropical North Atlantic (30–65°N) (top), and in a more muted fashion in the tropical Atlantic (10–20°N) SST anomalies. Both series come from HadSST2 (Rayner et al., 2006) and are relative to 1961–1990 mean (°C).

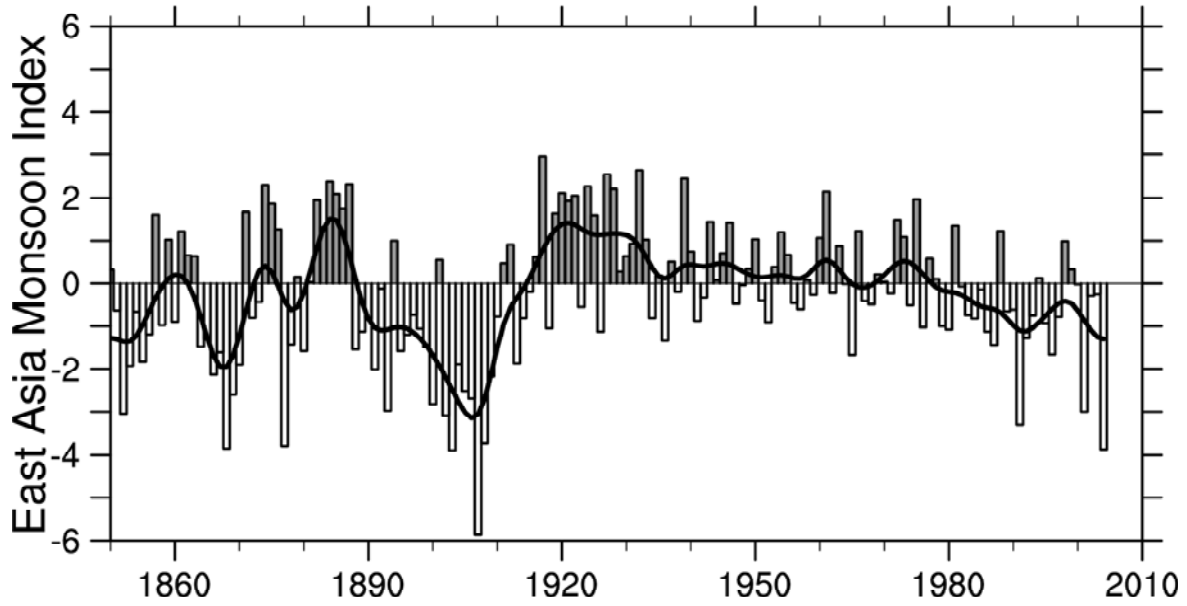
1
2



3
4
5
6
7
8
9
10
11

Figure 3.7.1. Change in the epoch mean annual range of precipitation: post-1976 epoch minus pre-1975 epoch in mm/day. Blue/green (red) colour denotes decreasing (increasing) annual range of the monsoon rainfall. Grey areas indicate missing values (oceans) or areas with insignificant annual changes. Data used are obtained from NCEP (PREC/L) (Data from Chen et al., 2002; see Wang and Ding, 2006).

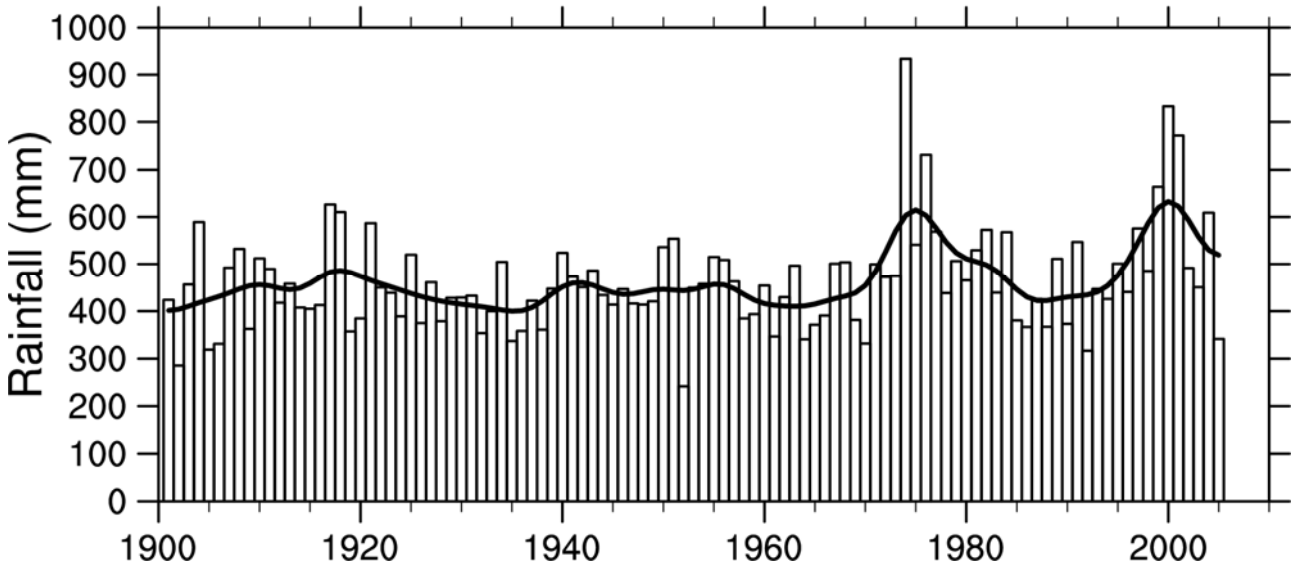
1
2



3
4
5
6
7
8
9

Fig 3.7.2. East Asia summer monsoon index derived from MSLP gradients between land and ocean in the east Asia region. The definition of the index is based on Guo et al. (2003) but was recalculated based on the HadSLP2 (Allan and Ansell, 2006) data set. Annual values are shown and the black smooth curve is the decadal filter (Appendix 3.A).

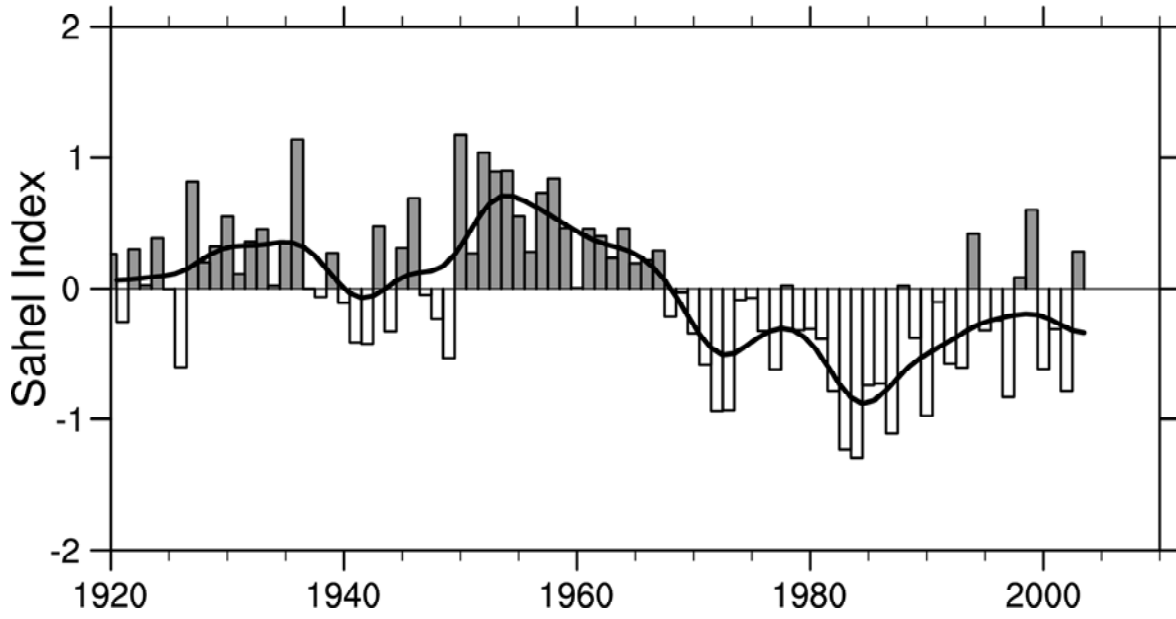
1
2



3
4
5
6
7
8
9

Figure 3.7.3. Time series of northern Australian (north of 26°S) wet-season (October–April) rainfall during 1900/1901 to 2004/2005. Individual years are plotted according to the date of the January. Black curve indicates the decadal filter (Appendix 3.A). Data from Australian Bureau of Meteorology.

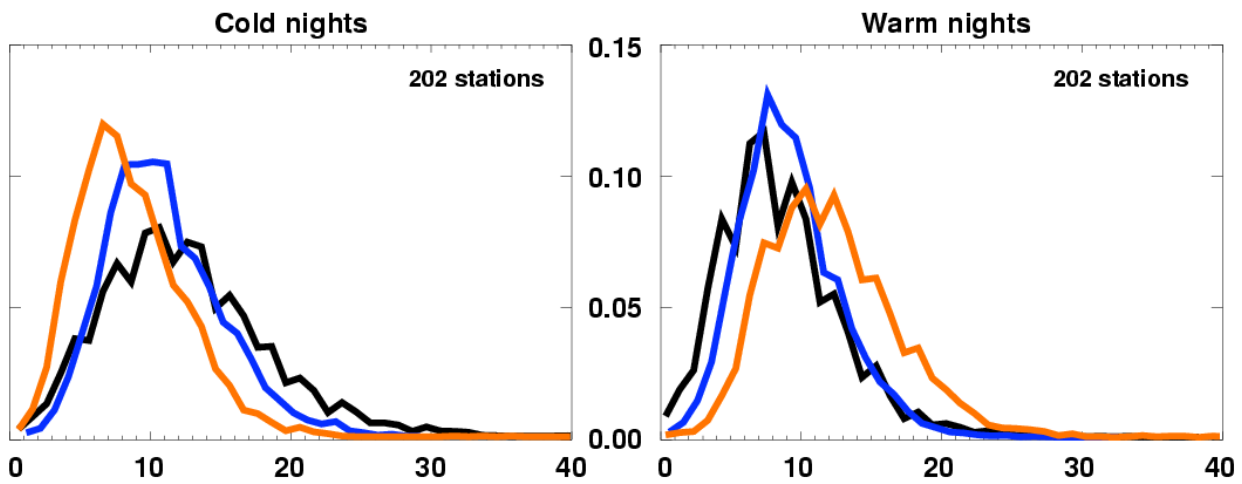
1
2



3
4
5
6
7
8
9

Figure 3.7.4. Time series of Sahel regional rainfall for April–October from 1920 to 2003 derived from gridding normalized station anomalies and then averaging using area weighting (adapted from Dai et al., 2004a). The decadal filter is from Appendix 3.A.

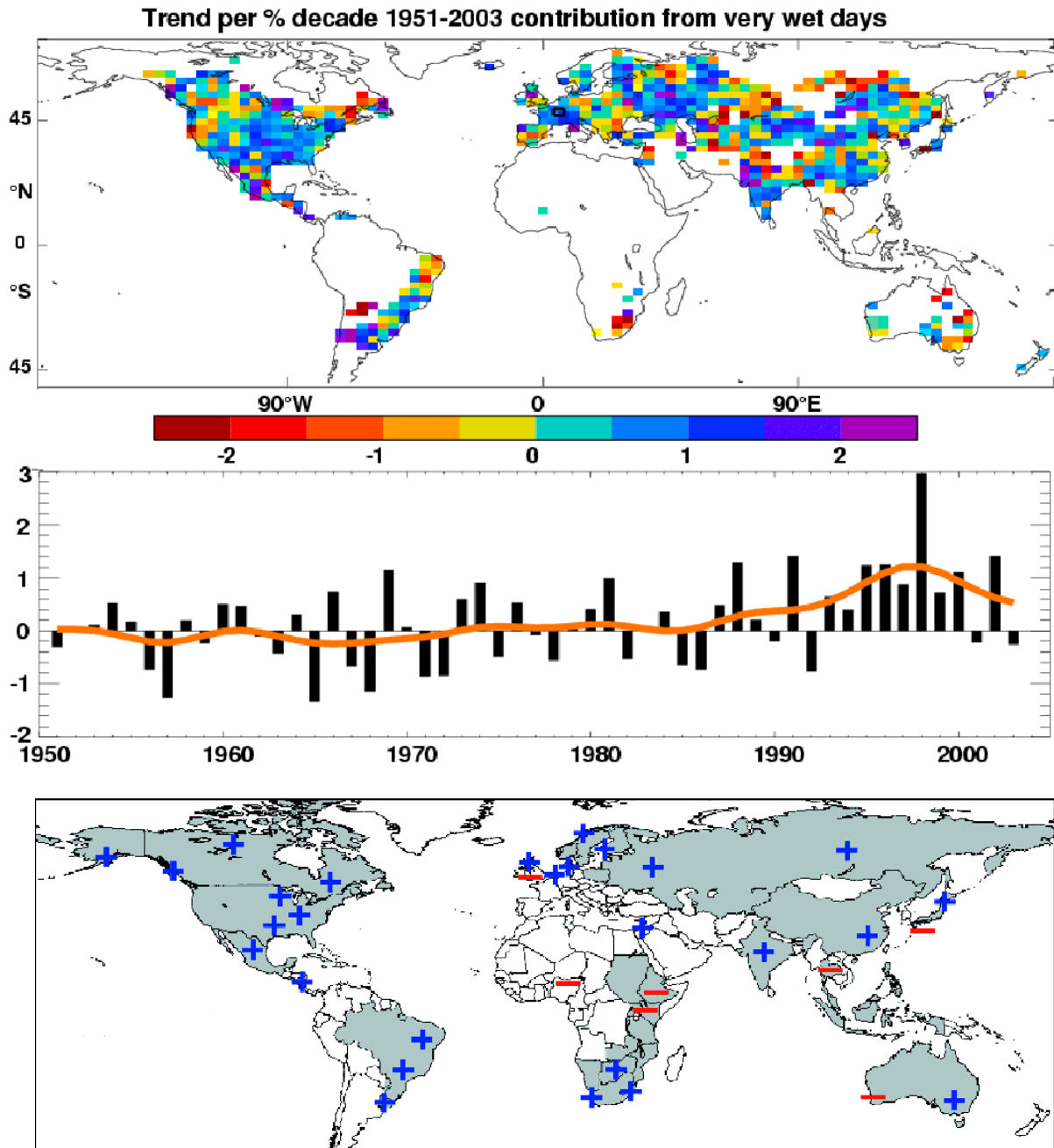
1
2



3
4
5
6
7
8
9
10
11

Figure 3.8.1. Annual probability density functions for temperature indices for 202 global stations with at least 80% complete data between 1901 and 2003 for 3 time periods: 1901–1950 (black), 1951–1978 (blue) and 1979–2003 (red). The x-axis represents the percentage of time during the year when the indicators were below the 10th percentile (left) for cold nights or above the 90th percentile (right) for warm nights. From Alexander et al. (2006).

1
2



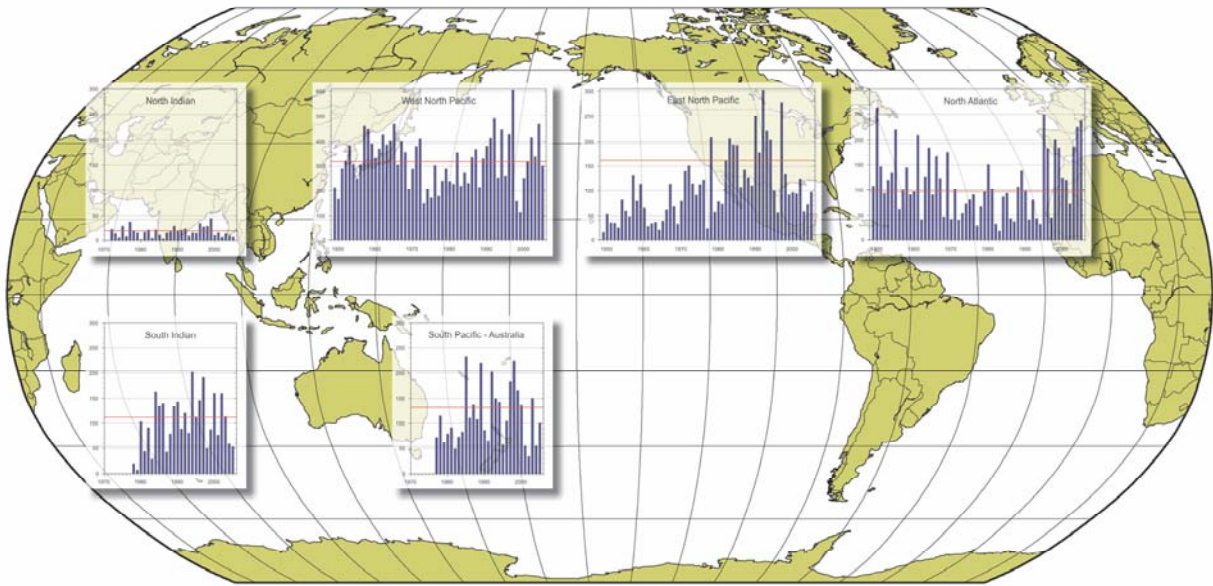
3
4

5
6

Figure 3.8.2. Upper: Observed trends (%) per decade for 1951–2003 for the contribution to total annual precipitation from very wet days corresponding to the 95th percentile. Trends were only calculated for grid boxes where both total and the 95th percentile had at least 40 years of data during this period and had data until at least 1999. Middle: Anomalies of the global annual time series (with respect to 1961–1990) defined as the percentage change from the base period average (22.5%). The red line shows decadal variations. From Alexander et al. (2006). Lower: Regions where disproportionate changes in heavy and very heavy precipitation during the past decades were documented compared to the change in the annual and/or seasonal precipitation (updated from Groisman et al., 2005a). Thresholds used to define “heavy” and “very heavy” precipitation vary by season and region. However, changes in heavy precipitation frequencies are always higher than changes in precipitation totals and, in some regions, an increase in heavy and/or very heavy precipitation occurred while no change or even a decrease in precipitation totals was observed.

18

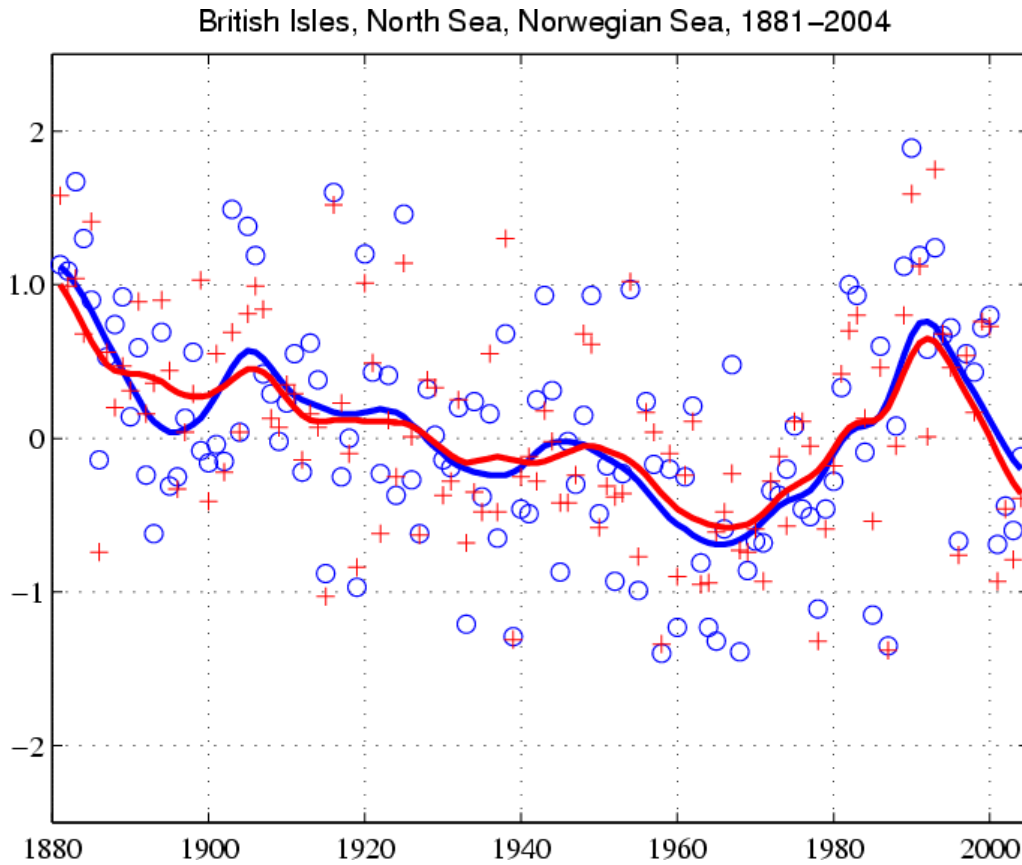
1
2



3
4
5
6
7
8
9
10
11
12

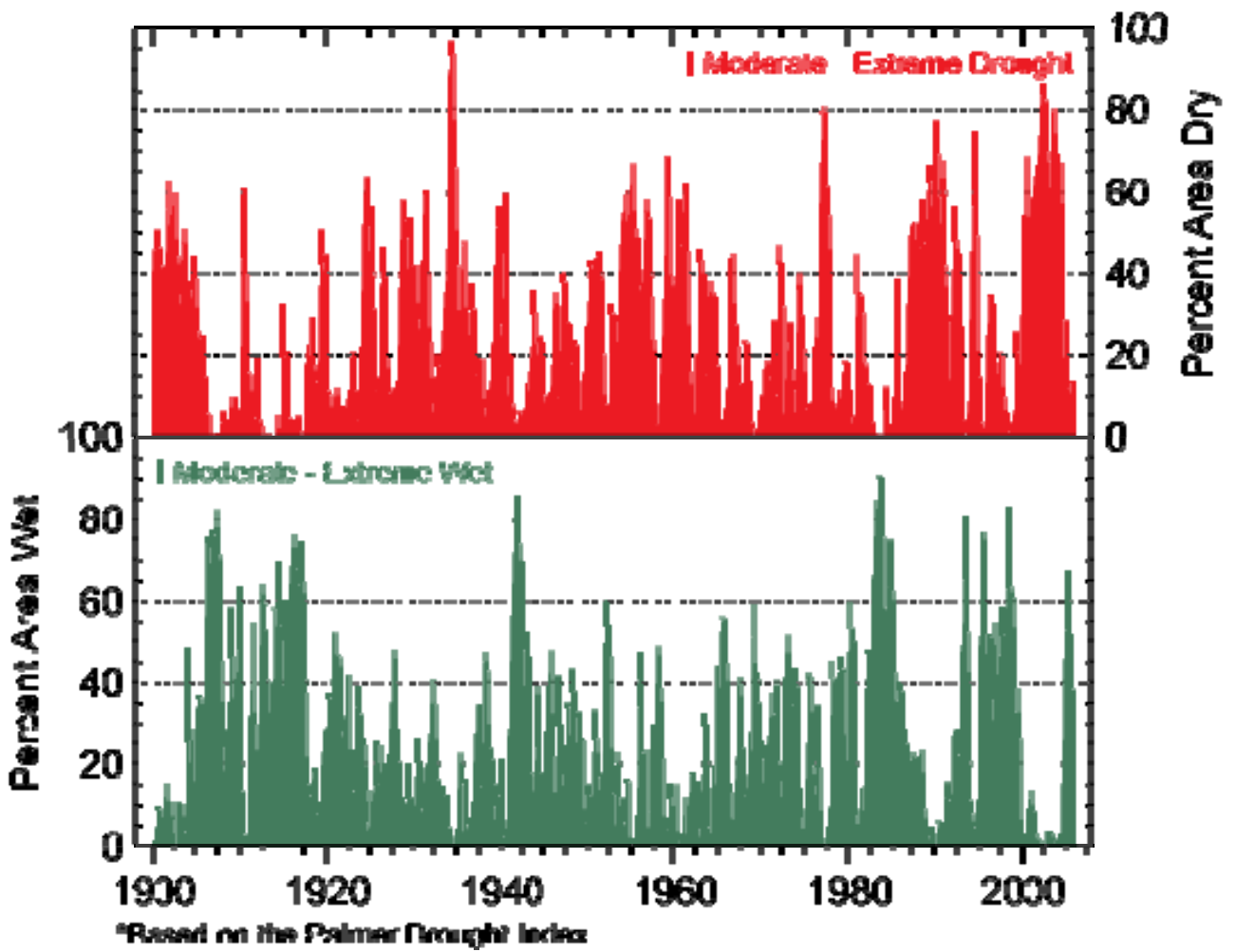
Figure 3.8.3. Seasonal values of the Accumulated Cyclone Energy (ACE) index for the North Indian, South Indian, West North Pacific, East North Pacific, North Atlantic and combined Australian-South Pacific regions. The vertical scale in the West N. Pacific is half that of other basins. The timeline runs from 1948 or 1970 through 2005. The SH values are those for the season from July the year before to June of the year plotted. The ACE index accounts for the combined strength and duration of tropical storms and hurricanes during a given season by computing the sum of squares of the 6-hour maximum sustained surface winds in knots while the storm is above tropical storm intensity. Adapted and updated from Levinson (2005).

1
2



3
4
5
6
7
8

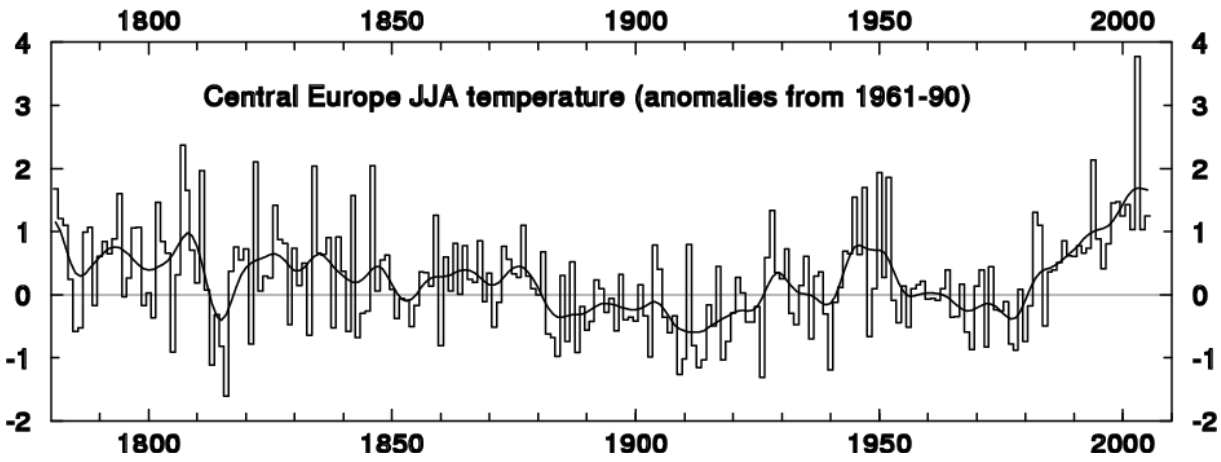
Figure 3.8.4. Storm index for British Isles, North Sea, Norwegian Sea, 1881–2004. Blue circles are 95th percentiles and red crosses 99th percentiles of standardized geostrophic winds averaged over 10 sets of triangles of stations. The smoothed curves are a decadal filter (updated from Alexandersson et al., 2000).



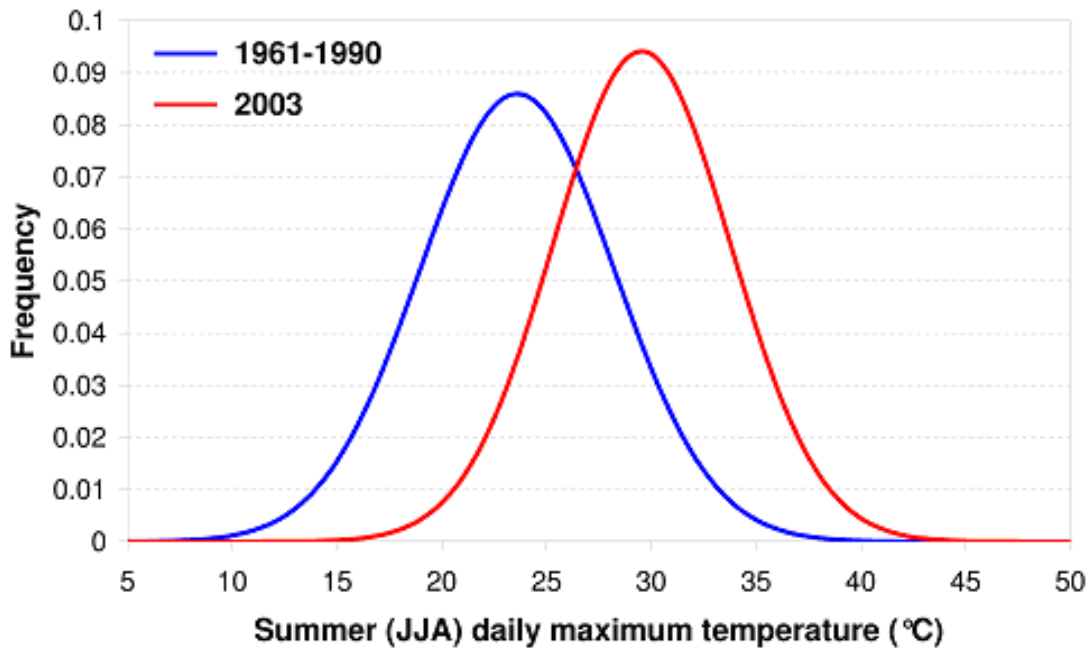
1
2
3
4
5
6

Box 3.6.3, Figure 3.8.5. Percentage of United States west of the Rocky Mountains dry (top) or wet (bottom) based on the Palmer Drought Severity Index for classes moderate to extreme drought or wet. From NOAA NCDC.

1



2



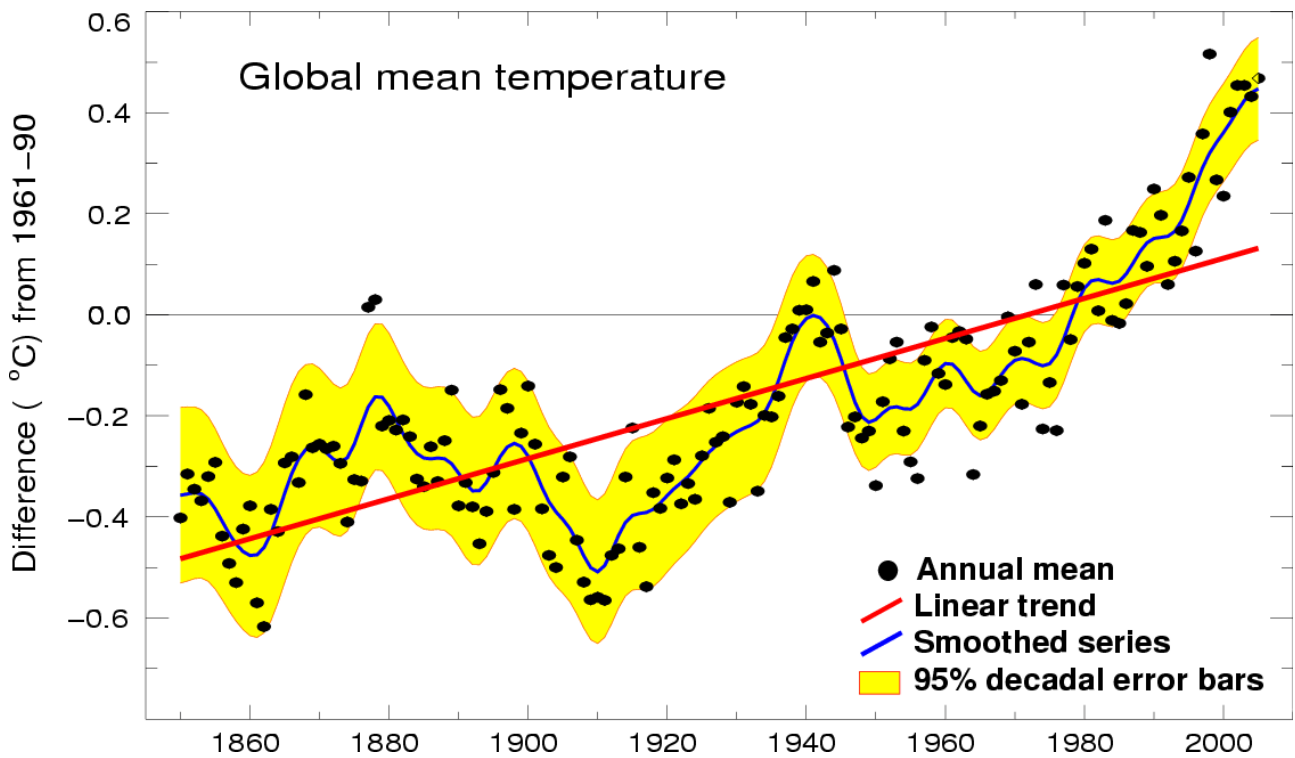
3

4

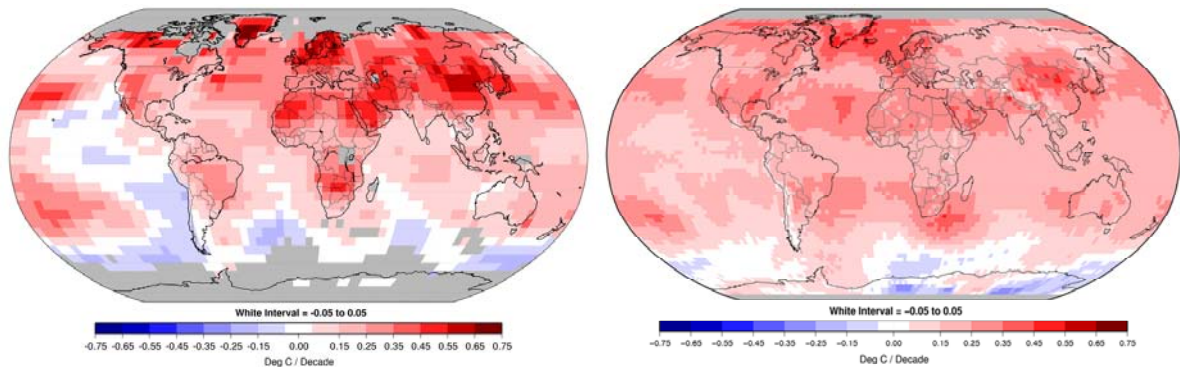
5 **Box 3.6.5, Figure 3.8.6.** Long time series of JJA temperature anomalies in Central Europe relative to 1961–
6 1990. In the summer of 2003 the value of 3.8°C far exceeded the next largest anomaly of 2.3°C in 1807, and
7 the highly smoothed Gaussian distribution (lower panel) of maximum temperatures (red) compared with
8 normal (blue) at Basel, Switzerland (Beniston and Diaz, 2004) shows how the whole distribution was
9 shifted.

10

1

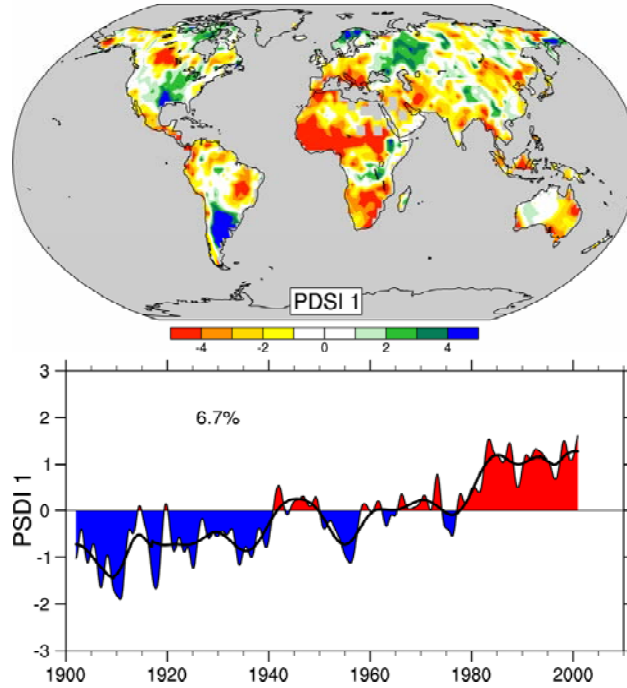


2
4
6
8



9 **Question 3.1, Figure 1.** *Top:* Annual global mean temperatures (black dots, from HadCRUT3) are given
 10 along with simple fits to the data. The red line is a linear trend fit to the complete 1850–2005 record. The
 11 blue curve is a smoothed depiction to capture the decadal variations, with decadal 95% (yellow) error range
 12 about that line (accordingly, annual values do exceed those limits). From model results (Chapter 9), there is
 13 little change prior to about 1920, and a substantial fraction of the early 20th century warming was
 14 contributed by naturally occurring influences including solar radiation changes, volcanism, and natural
 15 variability, from about 1940 to 1970 the increasing industrialization following World War II increased
 16 pollution in the NH contributing to cooling, but after the mid-1990s increases in carbon dioxide and other
 17 greenhouse gases are believed to dominate the observed warming. *Bottom:* Patterns of linear global
 18 temperature trends 1979 to 2005 estimated at the surface (left), and for the troposphere (from satellite
 19 records) (right). Grey areas indicate incomplete data.
 20

1
2

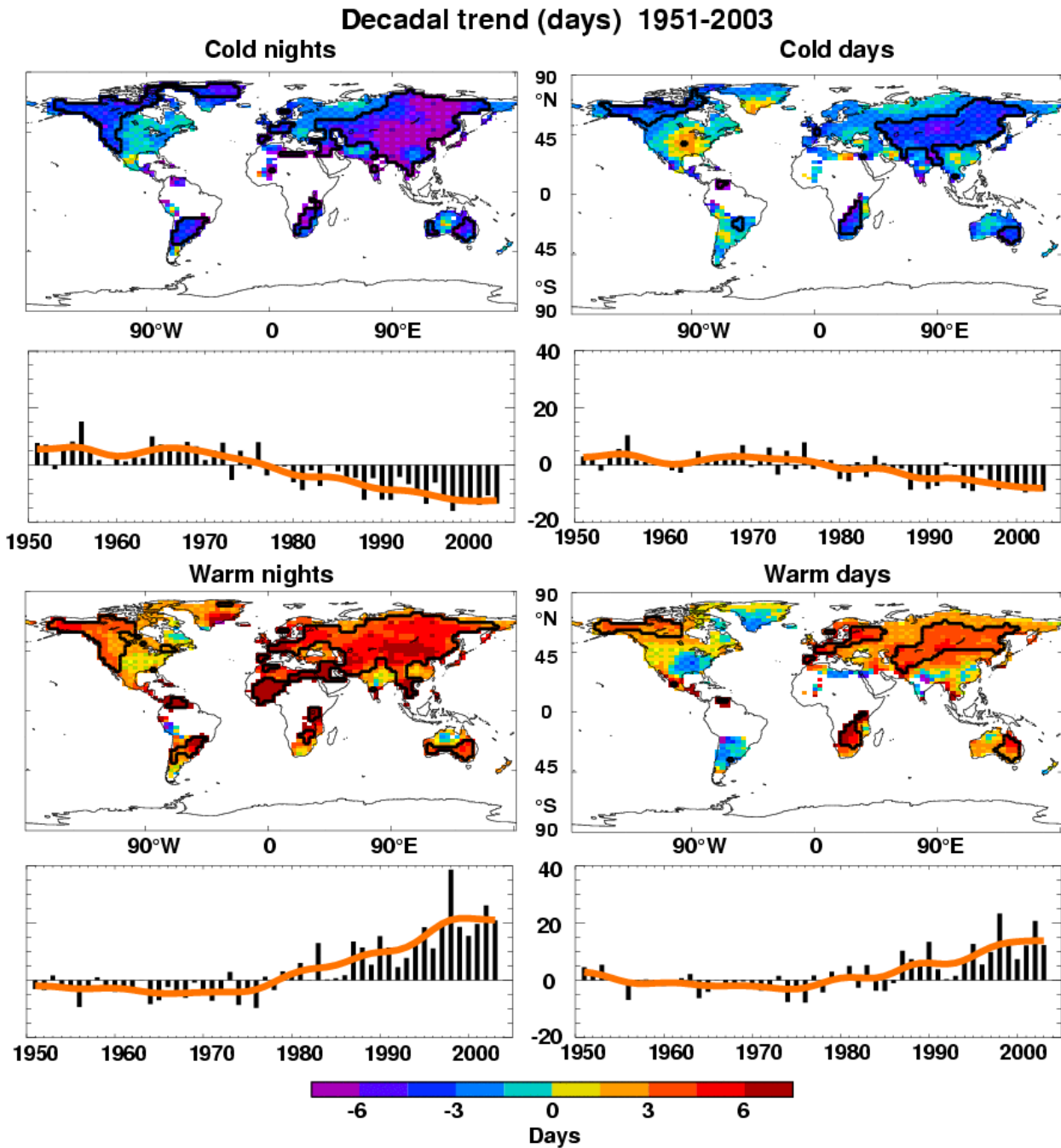


3

4
5
6
7
8
9
10
11

Question 3.2, Figure 1. The most important spatial pattern (top) of the monthly Palmer Drought Severity Index. Red and orange areas are drier than average and blue areas are wetter than average when the values shown in the lower plot are positive. The lower panel shows how the sign and strength of this pattern has changed since 1900. The time series (6.7% of variance) approximately corresponds to a trend and features the Sahel drought, for instance. Adapted from Dai et al. (2004b).

1
2



3
4
5
6
7
8
9
10
11
12

Question 3.3, Figure 1. Observed trends (days per decade) for 1951 to 2003 for the percentile temperature indices (a) cold nights, (b) cold days, (c) warm nights, and (d) warm days. Trends were only calculated for grid boxes that had at least 40 years of data during this period and had data until at least 1999. Black lines enclose regions where trends are significant at the 5% level. Below each map are the global annual time series anomalies (with respect to 1961–1990). The red line shows decadal variations. Trends are significant at the 5% level for all the indices shown. From Alexander et al. (2006).